 

https://doi.org/10.1070/QEL17044

# Quantum dot lasers with asymmetric barrier layers: Close-to-ideal threshold and power characteristics

L.V. Asryan

*Abstract.* **A theory of static (threshold and power) characteristics of novel diode lasers – quantum dot (QD) lasers with asymmetric barrier layers (ABLs) – is developed. The barrier layers are asymmetric in that they have considerably different heights for the carriers of opposite signs. The ABL located on the electron- (hole-) injecting side of the structure provides a low barrier (ideally no barrier) for electrons (holes) [so that it does not prevent electrons (holes) from easily approaching the active region] and a high barrier for holes (electrons) [so that holes (electrons) injected from the opposite side of the structure do not overcome it]. The use of ABLs should thus ideally prevent the simultaneous presence of electrons and holes (and hence parasitic electron–hole recombination) outside the QDs. It is shown in this work that in such a case of total suppression of parasitic recombination, the QD lasers with ABLs offer close-to-ideal performance: the threshold current density is below 10 A cm$^{-2}$ at any temperature, the absolute value of the characteristic temperature is above 1000 K (which manifests a virtually temperature-independent operation), the internal differential quantum efficiency is practically unity, and the light–current characteristic is linear at any pump current.**

***Keywords:*** *quantum dot lasers, semiconductor lasers.*

## 1. Introduction

In conventional diode lasers, pumping the active region (i.e., creating the population inversion required for lasing) is a three-step process. It includes injection of electrons and holes to the waveguide region [optical confinement layer (OCL)] from the cladding layers located on the opposite sides of this region, transportation through this region to the active region, and capture into the latter (Fig. 1a). Only a small fraction of electrons and holes injected to the OCL is finally captured into the active region – the majority of them remains in the OCL. Besides, electrons (holes) are easily transported to that side of the OCL where holes (electrons) are coming from (right- (left-) hand side in Fig. 1a). Hence, the carrier population is bipolar throughout the OCL. While simultaneous population of electrons and holes is required in the active region, bipolar population outside the active region is undesirable. In the presence of such population, electron–hole recombination occurs there [1–21]. This recombination is parasitic as it adversely affects the laser characteristics. In particular,

**L.V. Asryan** Virginia Polytechnic Institute and State University, Blacksburg, Virginia 24061, USA; e-mail: asryan@vt.edu

Received 22 April 2019
*Kvantovaya Elektronika* **49** (6) 522–528 (2019)
Submitted in English

(i) the fraction of injection current that goes into the parasitic electron–hole recombination is considerable; hence the threshold current is increased [8, 12, 13, 15, 18];

(ii) the parasitic recombination outside the active region presents a major source for the temperature dependence of the threshold current [8, 12, 13, 15, 18]; and

(iii) the parasitic recombination rate rises superlinearly with injection current above the lasing threshold, which leads to sublinearity of the light–current characteristic (LCC) and limits the output optical power [19–21].

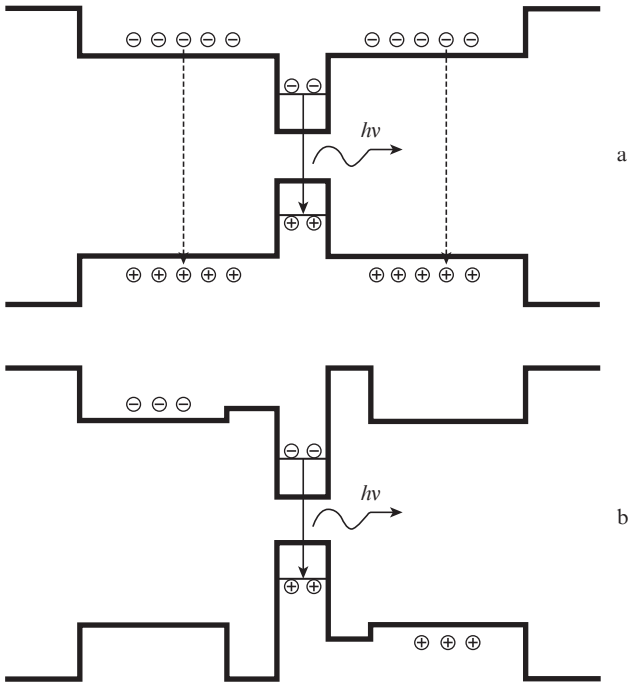


**Figure 1.** Energy band diagrams of (a) a conventional diode laser and (b) an ABL laser. The vertical solid arrows show the electron–hole recombination in the active region (QDs). The vertical dashed arrows show the parasitic electron–hole recombination outside the active region (in the OCL).

The use of asymmetric barrier layers (ABLs) was proposed [22, 23] as one of two approaches to suppress the recombination of electron–hole pairs outside a quantum-confined active region in semiconductor lasers. While the other approach – double tunneling-injection of charge carriers – was extensively discussed in the context of quantum dot (QD) lasers [22–31], the concept of ABLs was only applied to quantum well (QW) lasers so far [32–37]. A considerably higher tem-

perature stability of the threshold current was demonstrated in ABL QW lasers as compared to reference QW lasers without ABLs [33]. In the meantime, due to a truly discrete energy spectrum of carriers in QDs, still better characteristics are anticipated for ABL lasers, which will use a layer with QDs as the active region instead of a QW. This work explores the potential of ABL QD lasers for low-threshold, temperature-stable, and high-power operation.

In ABL QD lasers, to prevent bipolar population in the OCL and thus to suppress parasitic recombination there, the QD layer is sandwiched between two barrier layers. The layers are asymmetric – in the layer located on that side of the OCL into which electrons (holes) are injected [left- (right-) hand side in Fig. 1b], the energy barrier for electrons (holes) [i.e., the conduction (valence) band offset between the materials of the ABL and OCL] is low (ideally, zero) while that for holes (electrons) [i.e., the valence (conduction) band offset between the materials of the ABL and OCL] is high. Such asymmetry in the barrier heights for electrons and holes in each ABL will ensure that

(i) the carriers coming from that side of the structure, into which there were injected, will easily reach and be captured to the active region; and

(ii) the further transport of these carriers to the opposite side of the structure, i.e., to that side of the structure, into which the carriers of the opposite sign were injected, will be effectively blocked.

Assuming that the ABLs function ideally, there will be no bipolar population and hence parasitic electron–hole recombination in the OCL in the structure of Fig. 1b, electrons (holes) will not reach the right- (left-) hand side of the OCL. The only location in the structure, where the electrons and holes will meet together and recombine, will be the quantum-confined active region.

Asymmetric band structures and carrier blocking layers were discussed elsewhere (see, e.g., [38–46]) but for purposes other than suppression of the parasitic electron–hole recombination outside the active region.

## 2. Rate equations

To explore the potential of ABL QD lasers for low-threshold, temperature-stable, and high-power operation, it is assumed here that the ABLs function ideally, i.e.,

(i) the left-hand-side ABL totally blocks holes from entering the left-hand side of the OCL while not hindering at all the electron injection into QDs; and

(ii) the right-hand-side ABL totally blocks electrons from entering the right-hand side of the OCL while not hindering at all the hole injection into QDs.

The following set of rate equations is used, which includes all the main processes in the layered structure of Fig. 1b:
for free electrons in the left-hand side of the OCL,

$$b_1\frac{\partial n_{\rm L}}{\partial t}=\frac{j}{e}+\sigma_n v_n n_1 N_{\rm S} f_n-\sigma_n v_n n_{\rm L} N_{\rm S}(1-f_n) \tag{1}$$

for free holes in the right-hand side of the OCL,

$$b_2\frac{\partial p_{\rm R}}{\partial t}=\frac{j}{e}+\sigma_p v_p p_1 N_{\rm S} f_p-\sigma_p v_p p_{\rm R} N_{\rm S}(1-f_p) \tag{2}$$

for electrons and holes confined in QDs,

$$2N_{\rm S}\frac{\partial f_n}{\partial t}=\sigma_n v_n n_{\rm L} N_{\rm S}(1-f_n)-\sigma_n v_n n_1 N_{\rm S} f_n - N_{\rm S}\frac{f_n f_p}{\tau_{\rm QD}}-c_{\rm g}g^{\max}(f_n+f_p-1)n_{\rm ph}, \tag{3}$$

$$2N_{\rm S}\frac{\partial f_p}{\partial t}=\sigma_p v_p p_{\rm R} N_{\rm S}(1-f_p)-\sigma_p v_p p_1 N_{\rm S} f_p - N_{\rm S}\frac{f_n f_p}{\tau_{\rm QD}}-c_{\rm g}g^{\max}(f_n+f_p-1)n_{\rm ph} \tag{4}$$

and for photons,

$$\frac{\partial n_{\rm ph}}{\partial t}=c_{\rm g}g^{\max}(f_n+f_p-1)n_{\rm ph}-c_{\rm g}\beta n_{\rm ph.} \tag{5}$$

Here, $b_1$ ($b_2$) is the thickness of the left- (right-) hand side of the OCL [the separation between the n- (p-) cladding layer and the left- (right-) hand-side barrier (see Fig. 1b)]; $n_{\rm L}$ and $p_{\rm R}$ are the free-electron and -hole densities in the left- and right-hand sides of the OCL, respectively; $j$ is the injection current density; $e$ is the electron charge; $\sigma_{n,p}$ are the cross sections of electron and hole capture into a QD; $v_{n,p}$ are the electron and hole thermal velocities; $N_{\rm S}$ is the surface density of QDs; $f_{n,p}$ are the electron- and hole-level occupancies in QDs; $\tau_{\rm QD}$ is the spontaneous radiative lifetime in QDs; $c_{\rm g}$ is the group velocity of light in the cavity; $g^{\max}$ is the maximum value of the modal gain [8, 12, 15]; $\beta=(1/L)\ln(1/R)$ is the mirror loss coefficient; $L$ is the cavity length; $R$ is the facet reflectivity; and $n_{\rm ph}$ is the photon density (number of photons per unit area of the junction) in the lasing mode.

The quantities $n_1$ and $p_1$ in (1)–(4) characterise the intensities of electron and hole thermal escape from a QD to the OCL. They are given by

$$n_1=N_{\rm c}^{\rm 3D}\exp\left(-\frac{E_n}{T}\right),\quad p_1=N_{\rm v}^{\rm 3D}\exp\left(-\frac{E_p}{T}\right), \tag{6}$$

where $N_{\rm c,v}^{\rm 3D}=2[m_{\rm c,v}^{\rm OCL}T/(2\pi\hbar^2)]^{3/2}$ are the effective densities of states in the conduction and valence bands in the OCL; $m_{\rm c,v}^{\rm OCL}$ are the electron and hole effective masses in the OCL; $E_{n,p}$ are the electron and hole excitation energies from a QD to the OCL; and $T$ is the temperature (in units of energy).

The first term in the right-hand side in Eqn (1) [Eqn (2)] is the electron (hole) injection flux (in units of $\rm cm^{-2}\,s^{-1}$) from the n- (p-) cladding layer to the OCL. Each of these fluxes is given by the total injection current density $j$ divided by the electron charge: this reflects the fact that the current in the n- (p-) cladding layer (including the boundary with the OCL) is purely electron (hole) current.

The second term in the right-hand side in Eqn (1) [Eqn (2)] is the flux of thermal escape of electrons (holes) from QDs to the OCL and the third term is the flux of electron (hole) capture from the OCL into QDs.

In (3) and (4), $N_{\rm S}f_nf_p/\tau_{\rm QD}$ is the spontaneous radiative recombination flux in QDs. In (3)–(5), $c_{\rm g}g^{\max}(f_n+f_p-1)n_{\rm ph}$ is the flux of stimulated radiative recombination of electrons and holes in QDs, i.e., the flux of stimulated emission of photons. The second term in the right-hand side of (5) is the flux of photon escape from the cavity through the mirrors.

Adding up equations (1) and (3) gives

$$\frac{\partial}{\partial t}(b_1n_{\rm L}+2N_{\rm S}f_n)=\frac{j}{e}-N_{\rm S}\frac{f_nf_p}{\tau_{\rm QD}}-$$

$$- c_g g^{max}(f_n + f_p - 1)n_{ph}. \quad (7)$$

Adding up equations (2) and (4) gives

$$\frac{\partial}{\partial t}(b_2 p_R + 2N_S f_p) = \frac{j}{e} - N_S \frac{f_n f_p}{\tau_{QD}} - c_g g^{max}(f_n + f_p - 1)n_{ph}. \quad (8)$$

Subtracting Eqn (7) from Eqn (8) gives

$$\frac{\partial}{\partial t}[(b_2 p_R + 2N_S f_p) - (b_1 n_L + 2N_S f_n)] = 0. \quad (9)$$

Equation (9) is the condition of conservation of the total charge in the laser structure, which includes the charge of free electrons in the left-hand side of the OCL, free holes in the right-hand side of the OCL, and electrons and holes confined in QDs. Since the laser structure is not originally charged, the following condition of global charge neutrality is obtained from (9):

$$b_1 n_L + 2N_S f_n = b_2 p_R + 2N_S f_p. \quad (10)$$

Equality (10) simply states that the total charge of electrons in QDs and the left-hand side of the OCL is compensated for by the total charge of holes in QDs and the right-hand side of the OCL. As seen from (10), the local charge neutrality is violated in QDs, i.e., $f_n \neq f_p$ in the general case.

## 3. Steady-state characteristics

A GaInAsP heterostructure lasing near 1.55 μm is considered in this work [8, 12, 13, 15]. The materials of the cladding layers, OCL and QDs are InP, $Ga_{0.21}In_{0.79}As_{0.46}P_{0.54}$ and $Ga_{0.47}In_{0.53}As$, respectively, with the latter two being lattice-matched with InP. The cavity length is $L = 1.139$ mm (the mirror loss is $\beta = 10$ cm$^{-1}$), the width of the laser stripe is 2 μm, the surface density of the QD is $N_S = 6.11 \times 10^{10}$ cm$^{-2}$, and $T = 300$ K.

Continuous-wave operation is considered here and hence the rate equations (1)–(5) are solved at the steady state. At the steady state, the set of differential equations (1)–(5) reduces to the set of algebraic equations. As shown below, solving this set of algebraic equations reduces in turn to solving a single algebraic equation in one unknown [see Eqn (15)].

From Eqn (5) at the steady state, the lasing condition is obtained in the form (equality of the gain to the loss):

$$g^{max}(f_n + f_p - 1) = \beta. \quad (11)$$

From (11) and (1), $f_p$ and $n_L$ are expressed in terms of $f_n$ as follows:

$$f_p(f_n) = 1 + \frac{\beta}{g^{max}} - f_n, \quad (12)$$

$$n_L(f_n) = n_1 \frac{f_n}{1 - f_n} + \frac{j}{e\sigma_n v_n N_S(1 - f_n)}. \quad (13)$$

From (2) and using (12), $p_R$ is also expressed in terms of $f_n$,

$$p_R = p_1 \frac{f_p(f_n)}{1 - f_p(f_n)} + \frac{j}{e\sigma_p v_p N_S[1 - f_p(f_n)]} = p_1 \frac{1 + \beta/g^{max} - f_n}{f_n - \beta/g^{max}} + \frac{j}{e\sigma_p v_p N_S[f_n - \beta/g^{max}]}. \quad (14)$$

Substituting $f_p$, $n_L$, and $p_R$ from (12)–(14) into (10), the following equation is obtained to find $f_n$:

$$b_1\left[n_1 \frac{f_n}{1 - f_n} + \frac{j}{e\sigma_n v_n N_S(1 - f_n)}\right] + 2N_S f_n = b_2\left[p_1 \frac{1 + \beta/g^{max} - f_n}{f_n - \beta/g^{max}} + \frac{j}{e\sigma_p v_p N_S(f_n - \beta/g^{max})}\right] + 2N_S\left(1 + \frac{\beta}{g^{max}} - f_n\right). \quad (15)$$

Equation (15) can be rewritten as a cubic equation in $f_n$. Solving (15), $f_n$ is found and then, using (12)–(14), $f_p$, $n_L$, and $p_R$ are calculated.

As seen from (15) and (12) and shown in Fig. 2, $f_n$ and $f_p$ vary with injection current density $j$. The fact that the electron and hole level occupancies in QDs are not pinned in the lasing regime is entirely due to violation of local neutrality in QDs, i.e., to electron–hole asymmetry. Indeed, assuming local neutrality in QDs one would immediately obtain from (11) that $f_{n,p}$ are pinned at the same (threshold) value given by

$$f_n^{neutral} = f_p^{neutral} = \frac{1}{2}\left(1 + \frac{\beta}{g^{max}}\right), \quad (16)$$

and shown by the horizontal dashed line in Fig. 2.

From Eqn (7) [or (8)] at the steady-state and using (11), the photon density is calculated,

$$n_{ph}(j) = \tau_{ph} \frac{j - j_{spon}^{QD}(j)}{e}, \quad (17)$$

where $\tau_{ph} = 1/(c_g\beta)$ is the photon lifetime in the cavity and

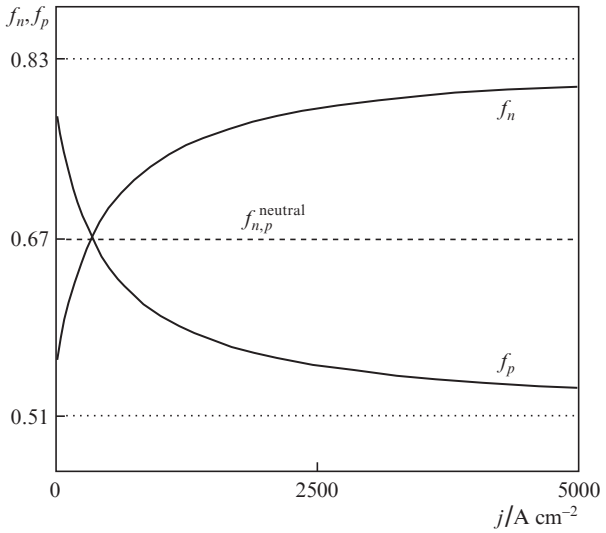


**Figure 2.** Electron and hole level occupancies in QDs vs. injection current density. The horizontal dashed line shows the electron and hole level occupancies calculated assuming local neutrality in QDs [Eqn (16)]. The horizontal dotted lines show the asymptotic values of the electron and hole level occupancies given by (29) and (30).

$$j_{\text{spon}}^{\text{QD}}(j) = eN_{\text{S}}\frac{f_n(j)f_p(j)}{\tau_{\text{QD}}} \tag{18}$$

is the spontaneous radiative recombination current density in QDs.

Finally, the current density of stimulated recombination, $j_{\text{stim}}$, and the output optical power of the laser, $P$, are calculated,

$$j_{\text{stim}}(j) = e\frac{n_{\text{ph}}(j)}{\tau_{\text{ph}}} = j - j_{\text{spon}}^{\text{QD}}(j), \tag{19}$$

$$P(j) = \hbar\omega\frac{n_{\text{ph}}(j)}{\tau_{\text{ph}}}S = \frac{\hbar\omega}{e}j_{\text{stim}}(j)S = \frac{\hbar\omega}{e}S[j - j_{\text{spon}}^{\text{QD}}(j)], \tag{20}$$

where $\hbar\omega$ is the photon energy, $S = WL$ is the cross section of the junction, and $W$ is the lateral size of the device.

The output power can be written as

$$P(j) = \frac{\hbar\omega}{e}S(j - j_{\text{th}})\eta_{\text{int}}(j), \tag{21}$$

where the threshold current density $j_{\text{th}}$ (the lowest pump current density, at which the lasing starts) is found as the root of the equation

$$j - j_{\text{spon}}^{\text{QD}}(j) = 0, \tag{22}$$

and $\eta_{\text{int}}$ is the internal differential quantum efficiency (efficiency of stimulated emission), which is defined as [47]

$$\eta_{\text{int}}(j) = \frac{j_{\text{stim}}(j)}{j - j_{\text{th}}} = \frac{j - j_{\text{spon}}^{\text{QD}}(j)}{j - j_{\text{th}}}. \tag{23}$$

If QDs were neutral, the optical power would be given by

$$P^{\text{neutral}} = \frac{\hbar\omega}{e}S(j - j_{\text{th}}^{\text{neutral}}), \tag{24}$$

with

$$j_{\text{th}}^{\text{neutral}} = eN_{\text{S}}\frac{(f_n^{\text{neutral}})^2}{\tau_{\text{QD}}} \tag{25}$$

being the threshold current density in that case. As seen from (24) and (25), under the condition of local neutrality in QDs, the LCC of ABL QD lasers (the output optical power versus the injection current density) is linear.

As seen from (17), (19), and (20), the only mechanism of non-stimulated recombination in an ideally functioning ABL QD laser is the spontaneous radiative recombination in QDs. Since the level occupancies in QDs $f_n(j)$ and $f_p(j)$ cannot exceed unity, the current density consumed by spontaneous radiative recombination in QDs [see (18)] also remains limited,

$$j_{\text{spon}}^{\text{QD}}(j) \leqslant \frac{eN_{\text{S}}}{\tau_{\text{QD}}}. \tag{26}$$

For typical values of the surface density of QDs $N_{\text{S}}$ ($< 10^{11}$ cm$^{-2}$) and spontaneous radiative recombination time in QDs $\tau_{\text{QD}}$ ($\approx$ 1ns), the upper limit for the spontaneous recombination current density $eN_{\text{S}}/\tau_{\text{QD}}$ is less than 20 A cm$^{-2}$, which is a very low value. This means that, no matter what are the particular functional dependences of $f_n$ and $f_p$ on $j$, for the pump current density $j \gg eN_{\text{S}}/\tau_{\text{QD}}$, the spontaneous recombination current density in QDs can be safely neglected compared to $j$ in (20) thus yielding a linear LCC (Fig. 3),

$$P(j) = \frac{\hbar\omega}{e}jS. \tag{27}$$

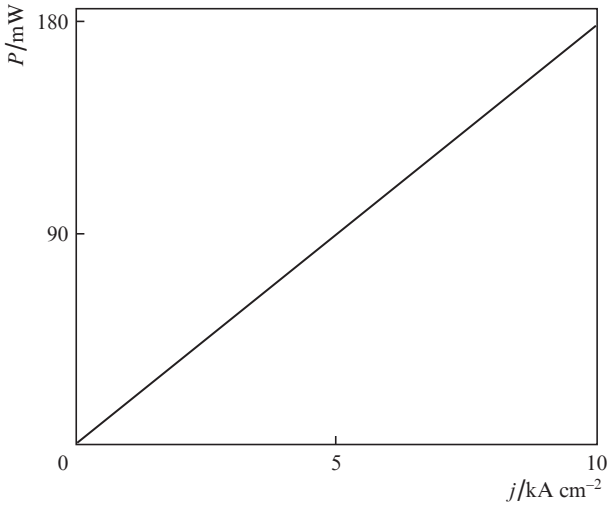


**Figure 3.** Light–current characteristic of an ABL QD laser: output optical power vs. injection current density; $T$= 300 K.

As seen from (21) and (27), the internal differential quantum efficiency $\eta_{\text{int}}$ is practically equal to unity.

As it might be concluded from (20) and (18), due to violation of local neutrality in QDs and the fact that $f_n$ and $f_p$ are nonlinear functions of the injection current density (Fig. 2), the LCC should also be nonlinear at low $j$, i. e., at $j$ slightly above $j_{\text{th}}$. However, even at low $j$, the LCC of ABL lasers is virtually linear and very close to that given by Eqn (24) for the case of neutral QDs. The physics behind this is as follows. To satisfy the lasing condition (11), the sum $f_n + f_p$ should remain constant. With (11) and (16), this sum can be written us

$$f_n + f_p = 2f_{n,p}^{\text{neutral}}. \tag{28}$$

What this means is the increase in $f_n$ with $j$ is compensated for by the decrease in $f_p$ (Fig. 2). Hence, while the electron and hole level occupancies in QDs significantly vary with $j$, their product, which determines the spontaneous radiative recombination current density in QDs [see (18)], is almost constant and hence is not significantly affected by violation of local neutrality in QDs (Fig. 4). As a result of this, so is the LCC of the laser even at low $j$.

As seen from Fig. 2, $f_n$ and $f_p$ saturate with increasing $j$. From (15) and (12), the following expressions are obtained for the asymptotic values of $f_n$ and $f_p$ at $j \to \infty$ (the dotted horizontal lines in the figure):

$$f_{n,\text{asympt}} = \frac{\beta/g^{\max} + \tau_{p,\text{capt},0}/\tau_{n,\text{capt},0}}{1 + \tau_{p,\text{capt},0}/\tau_{n,\text{capt},0}}, \tag{29}$$

$$f_{p,\text{asympt}} = \frac{\beta/g^{\max} + \tau_{n,\text{capt},0}/\tau_{p,\text{capt},0}}{1 + \tau_{n,\text{capt},0}/\tau_{p,\text{capt},0}}, \tag{30}$$

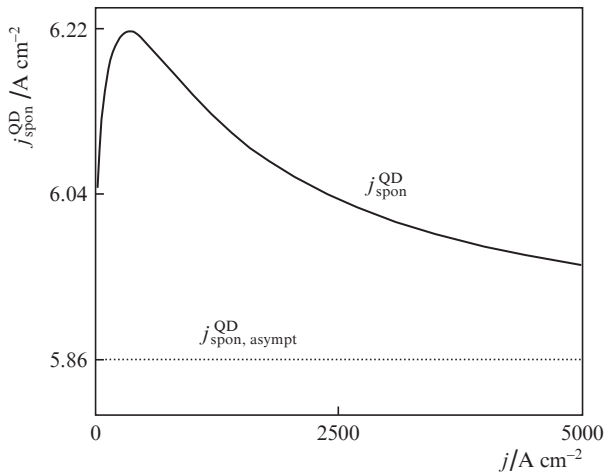


**Figure 4.** Spontaneous radiative recombination current density in QDs vs. injection current density. The horizontal dotted line shows the asymptotic value $j_{spon,asympt}^{QD} = (eN_S/\tau_{QD})f_{n,asympt}f_{p,asympt}$, where $f_{n,asympt}$ and $f_{p,asympt}$ are given by (29) and (30); $T = 300$ K.

where

$$\tau_{n,capt,0} = b_1/v_{n,capt,0}, \quad \tau_{p,capt,0} = b_2/v_{p,capt,0} \tag{31}$$

are the capture times of electrons and holes from the left- and right-hand sides of the OCL, respectively, into an empty QD ensemble (when $f_{n,p} = 0$). In (31), $v_{n,capt,0}$ and $v_{p,capt,0}$ are the capture velocities (in units of cm s$^{-1}$) into an empty QD ensemble given by [19–21]

$$v_{n,capt,0} = \sigma_n v_n N_S, \quad v_{p,capt,0} = \sigma_p v_p N_S. \tag{32}$$

While $f_n$ and $f_p$ differ considerably from each other, the free electron density $n_L$ in the left-hand side of the OCL is almost the same as the free hole density $p_R$ in the right-hand side of the OCL in the case of $b_1 = b_2$ considered here (Fig. 5). This is because each of the electron and hole charges (per unit area) confined in all QDs, $2N_S f_n$ and $2N_S f_p$, is negligible compared to the free-electron and -hole charges in the left- and right-hand sides of the OCL, $b_1 n_L$ and $b_2 p_R$.

Using (29) and (30) in (13) and (14), the following expressions are obtained for the asymptotic values of $n_L$ and $p_R$ at $j \to \infty$:

$$b_1 n_{L,asymp} = b_2 p_{R,asympt} = \frac{\tau_{n,capt,0} + \tau_{p,capt,0}}{1 - \beta/g^{max}} \frac{j}{e}. \tag{33}$$

While the threshold current density for the case of neutral QDs is given by a closed-form expression [see (25)], no such expression can be derived for the case of charged QDs. However, the upper limit for $j_{th}$ can be easily found in the general case. As seen from (22), since $j_{spon}^{QD}$ is limited [see (26)], $j_{th}$ is limited as well and the upper limit for the latter is the same as that for $j_{spon}^{QD}$,

$$j_{th} \leqslant eN_S/\tau_{QD}. \tag{34}$$

As with the dependence on the injection current density, violation of local neutrality in QDs leads to the temperature-dependence of $f_n$ and $f_p$ (see [12, 13, 15] where this has been considered in the context of conventional QD lasers). If QDs were neutral, $f_{n,p}$ [see (16)] and hence the threshold current density [see (25)] would be independent of temperature. Accordingly, the characteristic temperature (a figure of merit of a diode laser from the viewpoint of temperature-stability of $j_{th}$) defined as

$$T_0 = \left(\frac{\partial \ln j_{th}}{\partial T}\right)^{-1}, \tag{35}$$

would be infinitely high.

As seen from (15), primarily due to exponential [see (6)] temperature dependences of $n_1$ and $p_1$ [the $T$-dependence of the electron and hole thermal velocities $v_{n,p}$ also entering into (15) is much weaker compared to these], $f_n$ should be temperature-dependent as well. Hence, so should be $f_p$ [see (12)]. Similarly to the dependences on the injection current density (Fig. 2), since the sum $f_n + f_p$ should remain constant [see (28)], to satisfy the lasing condition (11), the increase in $f_n$

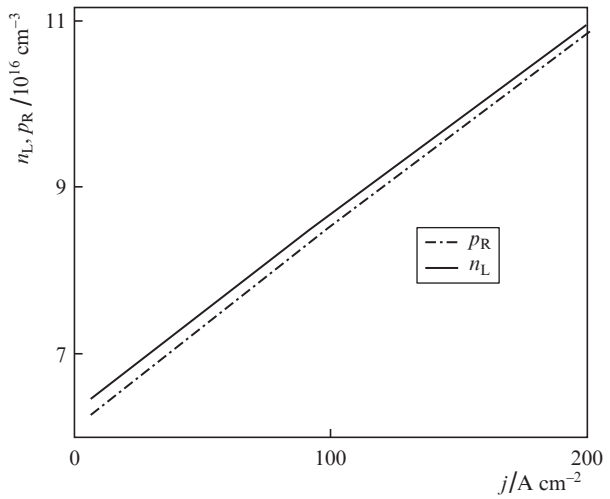


**Figure 5.** Free-electron density in the left hand side of the OCL and free-hole density in the right hand side of the OCL vs. injection current density; $T = 300$ K.

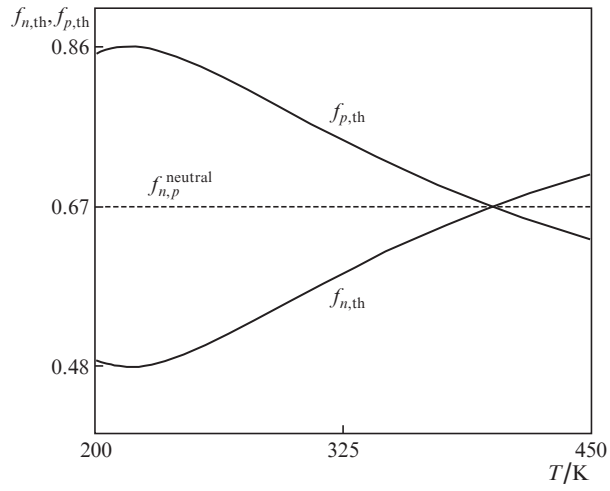


**Figure 6.** Electron and hole level occupancies in QDs at the lasing threshold vs. temperature. The horizontal dashed line shows the electron and hole level occupancies calculated assuming local neutrality in QDs [Eqn (16)].

with $T$ is compensated for by the decrease in $f_p$ (Fig. 6). As a result of this, the spontaneous recombination current density in QDs $j_{th}$, controlled by the product of $f_n$ and $f_p$ [see (18)], and hence the threshold current density $j_{th}$ [determined from (22)], vary only slightly with temperature varying in a wide range (Fig. 7). As seen from Fig. 7, $j_{th}$ is below 10 A cm$^{-2}$ in the entire temperature range from 200 to 450 K. As also seen from the figure, the temperature dependence of $j_{th}$ is nonmonotonous: with increasing temperature, $j_{th}$ first decreases, then increases, and then decreases again. Hence the characteristic temperature $T_0$ twice changes its sign: it is first negative, then positive, and then negative again (Fig. 8). At the temperatures, at which $j_{th}$ is at its minimum and maximum (217 and 401 K, respectively), the characteristic temperature is infinitely high ($T_0 = \infty$): $1/T_0 = 0$ at these temperatures in Fig. 8. As seen from Fig. 8, the absolute value of $T_0$ is above 1100 K in the entire temperature range. Such high values of $T_0$ in ABL lasers with charged QDs represent virtually temperature-independent $j_{th}$ for any practical applications.

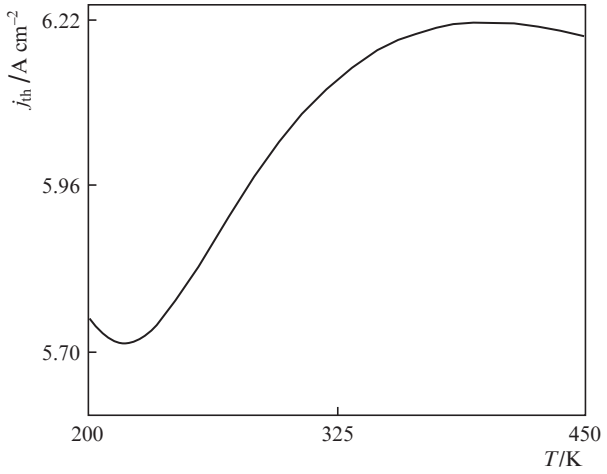


**Figure 7.** Threshold current density of an ABL QD laser vs. temperature.

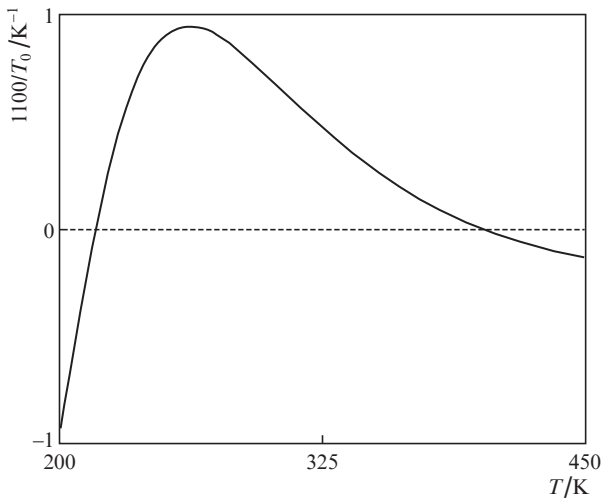


**Figure 8.** Reciprocal of the characteristic temperature of an ABL QD laser (multiplied by 1100) vs. temperature. The horizontal dashed line shows the reciprocal of the characteristic temperature calculated assuming local neutrality in QDs ($T_0^{neutral} = \infty$). At $T = 217$ K, $f_{n,th}$ is at its minimum and $f_{p,th}$ is at its maximum (see Fig. 6), $j_{th}$ is at its minimum (see Fig. 7), and hence [see (35)] $1/T_0 = 0$. At $T = 401$ K, $f_{n,th} = f_{p,th} = f_{n,p}^{neutral}$ (see Fig. 6), $j_{th}$ is now at its maximum (see Fig. 7), and hence $1/T_0$ is again equal to zero.

## 4. Conclusions

A theory of static characteristics of novel semiconductor lasers – QD lasers with ABLs – has been developed. Assuming that the ABLs function ideally, i. e., they completely block the simultaneous presence of electrons and holes outside the QDs, and hence the parasitic electron–hole recombination is totally suppressed there, it has been shown that the QD lasers with ABLs offer close-to-ideal performance: the threshold current density is below 10 A cm$^{-2}$ at any temperature, the absolute value of the characteristic temperature is above 1000 K (which manifests a virtually temperature-independent operation), the internal differential quantum efficiency is practically equal to unity, and the LCC is linear at any pump current.

***Acknowledgements.*** This work was supported by the U.S. Army Research Office (Grant No. W911NF-17-1-0432).

## References

1. Garbuzov D.Z., Ovchinnikov A.V., Pikhtin N.A., Sokolova Z.N., Tarasov I.S., Khalfin V.B. *Sov. Phys. Semicond.*, **25** (5), 560 (1991) [*Fiz. Tekh. Poluprovodn.*, **25** (5), 928 (1991)].
2. Rideout W., Sharfin W.F., Koteles E.S., Vassell M.O., Elman B. *IEEE Photon. Technol. Lett.*, **3** (9), 784 (1991).
3. Tessler N., Nagar R., Eisenstein G., Chandrasekhar S., Joyner C.H., Dentai A.G., Koren U., Raybon G. *Appl. Phys. Lett.*, **61** (20), 2383 (1992).
4. Hirayama H., Yoshida J., Miyake Y., Asada M. *Appl. Phys. Lett.*, **61** (20), 2398 (1992).
5. Zory P.S. Jr. *Quantum Well Lasers* (Boston: Academic, 1993).
6. Temkin H., Coblentz D., Logan R.A., Vandenberg J.M., Yadvish R.D., Sergent A.M. *Appl. Phys. Lett.*, **63** (17), 2321 (1994).
7. Evans J.D., Simmons J.G., Thompson D.A., Puetz N., Makino T., Chik G. *IEEE J. Sel. Top. Quantum Electron.*, **1** (2), 275 (1995).
8. Asryan L.V., Suris R.A. *Semicond. Sci. Technol.*, **11** (4), 554 (1996).
9. Seki S., Oohashi H., Sugiura H., Hirono T., Yokoyama K. *IEEE J. Quantum Electron.*, **32** (8), 1478 (1996).
10. Garbuzov D., Xu L., Forrest S.R., Martinelli R., Connolly J.C. *Electron. Lett.*, **32** (18), 1717 (1996).
11. Mawst L.J., Bhattacharya A., Lopez J., Botez D., Garbuzov D.Z., DeMarco L., Connolly J.C., Jansen M., Fang F., Nabiev R.F. *Appl. Phys. Lett.*, **69** (11), 1532 (1996).
12. Asryan L.V., Suris R.A. *IEEE J. Sel. Top. Quantum Electron.*, **3** (2), 148 (1997).
13. Asryan L.V., Suris R.A. *Electron. Lett.*, **33** (22), 1871 (1997).
14. Kazarinov R.F., Shtengel G.E. *J. Lightwave Technol.*, **15** (12), 2284 (1997).
15. Asryan L.V., Suris R.A. *IEEE J. Quantum Electron.*, **34** (5), 841 (1998).
16. Kapon E. *Semiconductor Lasers: Fundamentals* (New York: Academic, 1999).
17. Asryan L.V., Suris R.A. *Appl. Phys. Lett.*, **74** (9), 1215 (1999).
18. Asryan L.V., Gun'ko N.A., Polkovnikov A.S., Zegrya G.G., Suris R.A., Lau P.-K., Makino T. *Semicond. Sci. Technol.*, **15** (12), 1131 (2000).
19. Asryan L.V., Luryi S., Suris R.A. *Appl. Phys. Lett.*, **81** (12), 2154 (2002).
20. Asryan L.V., Luryi S., Suris R.A. *IEEE J. Quantum Electron.*, **39** (3), 404 (2003).
21. Asryan L.V., Sokolova Z.N. *J. Appl. Phys.*, **115** (2), 023107 (2014).

22. Asryan L.V., Luryi S. *Solid-State Electron.*, **47** (2), 205 (2003).
23. Asryan L.V., Luryi S. U.S. Patent No. 6,870,178, Mar. 22, 2005.
24. Asryan L.V., Luryi S. *IEEE J. Quantum Electron.*, **37** (7), 905 (2001).
25. Han D.-S., Asryan L.V. *Appl. Phys. Lett.*, **92** (25), 251113 (2008).
26. Han D.-S., Asryan L.V. *Solid-State Electron.*, **52** (10), 1674 (2008).
27. Han D.-S., Asryan L.V. *J. Lightwave Technol.*, **27** (24), 5775 (2009).
28. Han D.-S., Asryan L.V. *Nanotechnology*, **21** (1), 015201 (2010).
29. Asryan L.V. *Semicond. Sci. Technol.*, **30** (3), 035022 (2015).
30. Asryan L.V. *Opt. Lett.*, **42** (1), 97 (2017).
31. Asryan L.V., Kar S. *IEEE J. Quantum Electron.*, **55** (1), 2000109 (2019).
32. Asryan L.V., Kryzhanovskaya N.V., Maximov M.V., Egorov A.Yu., Zhukov A.E. *Semicond. Sci. Technol.*, **26** (5), 055025 (2011).
33. Zhukov A.E., Kryzhanovskaya N.V., Zubov F.I., Shernyakov Y.M., Maximov M.V., Semenova E.S., Yvind K., Asryan L.V. *Appl. Phys. Lett.*, **100** (2), 021107 (2012).
34. Asryan L.V., Kryzhanovskaya N.V., Maximov M.V., Zubov F.I., Zhukov A.E. *J. Appl. Phys.*, **114** (14), 143103 (2013).
35. Zubov F.I., Zhukov A.E., Shernyakov Y.M., Maximov M.V., Semenova E.S., Asryan L.V. *J. Phys. Conf. Ser.*, **643**, 012042 (2015).
36. Asryan L.V., Zubov F.I., Kryzhanovskaya N.V., Maximov M.V., Zhukov A.E. *Semicond.*, **50** (10), 1362 (2016) [*Fiz. Tekh. Poluprovodn.*, **50** (10), 1380 (2016)].
37. Asryan L.V., Zubov F.I., Balezina (Polubavkina) Yu.S., Moiseev E.I., Muretova M.E., Kryzhanovskaya N.V., Maximov M.V., Zhukov A.E. *Semicond.*, **52** (12), 1621 (2018) [*Fiz. Tekh. Poluprovodn.*, **52** (12), 1518 (2018)].
38. Kazarinov R.F., Belenky G.L. *IEEE J. Quantum Electron.*, **31** (3), 423 (1995).
39. Mawst L.J., Botez D. *Proc. SPIE*, **3001**, 7 (1997).
40. Ishizaka S., Muro K., Fujimoto T., Yamada Y. U.S. Patent No. 5764668, June 9, 1998.
41. Tomita A. U.S. Patent No. 6014394, Jan. 11, 2000.
42. He X. U.S. Patent No. 6298077 B1, Oct. 2, 2001.
43. Wiedmann N., Schmitz J., Boucke K., Herres N., Wagner J., Mikulla M., Poprawe R., Weimann G. *IEEE J. Quantum Electron.*, **38** (1), 67 (2002).
44. Lee J.J., Mawst L.J., Botez D. *J. Cryst. Growth*, **249**, 100 (2003).
45. Pataro L.L., Deng Y., Dapkus P.D. *Proc. IEEE LEOS 17th Annual Meeting* (Puerto Rico, 2004) Vol. 2, pp 469–470.
46. Liang R., Hosoda T., Kipshidze G., Shterengas L., Belenky G. *IEEE Photon. Technol. Lett.*, **25** (10), 925 (2013).
47. Coldren L.A., Corzine S.W. *Diode Lasers and Photonic Integrated Circuits* (New York: Wiley, 1995).